PAPER

Check for updates

Facile fabrication of zinc oxide coated superhydrophobic and superoleophilic meshes for efficient oil/water separation†

Yuezhong Zhang, [ID] *[a] Xiaoyu Wang,[b] Chunhui Wang,[b] Jiangjiang Liu,[b] Hongbiao Zhai,[b] Baosheng Liu,*[b] Xudong Zhao[a] and Daqing Fang[b]

Zinc oxide (ZnO) coated superhydrophobic and superoleophilic stainless steel meshes are facilely fabricated *via* chemical immersion growth and subsequent surface modification. The as-prepared meshes show good mechanical durability, chemical stability and corrosion-resistant properties due to a combination of the hierarchical ZnO structure and the low surface energy modification. More importantly, the as-prepared meshes are used for highly efficient separation of various oil/water mixtures. Meanwhile, a new oil skimmer based on the as-prepared mesh is proposed to spontaneously collect floating oil with high separation efficiency and desirable durability.

Introduction

Oily wastewater has become a serious world-wide environmental problem resulting from untreated industrial wastewater, sanitary wastewater and oil spillage accidents.[1–4] Therefore, it is necessary and imperative to develop some facile, highly-efficient and inexpensive technologies to assistant in the treatment and purification of oily wastewater.

Inspired by nature, the exploration and development of novel separation membranes with special wettability is deemed to be facile and effective.[5,6] In recent years, superwettable membranes (superhydrophobicity/superoleophilicity[7–10] or superhydrophilicity/underwater superoleophobicity[11–15]) have been used to separate oil/water mixtures utilizing the opposite wettability of the oil and water phases. Therefore, exploration of various oil/water separation membranes based on special wettability has become a popular topic. Recently, porous metal materials, such as copper mesh, steel mesh and nickel foam, have been widely investigated as promising substrates for separating oil from sewage.[16–18] Among the investigated porous metal materials, stainless steel mesh has gained special attention owing to its being cost-effective, and having high strength, flexibility and direct application in industry. As is well known, both constructing micro–nano scale structures and modification by low surface energy material are essential for fabricating

superhydrophobic surface on stainless steel meshes. Despite a number of methods have been proposed, facile construction of micro- and nanostructures on stainless steel mesh substrate for efficient oil/water separation is still a challenge.

Recently, ZnO, as a structural material, especially microstructures and nanostructures are popularly employed to fabricate special wettability surface due to its special physical and chemical properties. For example, Chen *et al.* applied femtosecond laser method to fabricate directly ZnO superhydrophobic surface on Zn substrate.[19] Huang *et al.* reported a superhydrophobic ZnO thin film on aluminum alloy substrate *via* electrodeposition method.[20] Velayi *et al.* fabricated superhydrophobic ZnO surfaces with reversible wettability.[21] Furthermore, some different approaches have been also reported to prepare ZnO micro/nanostructures on stainless steel mesh, such as electrodeposition,[22,23] sol–gel[24,25] and chemical vapor deposition.[23] However, most of the methods have limitations in practical fabrication, especially for large-scale fabrication, owing to complicated processes, expensive raw materials, and sophisticated equipment.

In this paper, we developed a simple, inexpensive and scalable approach to fabricate superhydrophobic and superoleophilic surface on the stainless steel meshes *via* ZnO microstructures construction process and low surface energy modification process. The as-prepared mesh exhibits good mechanical durability, chemical stability and corrosion-resistant properties. The as-prepared mesh can be used for separating various oil/water mixtures solely driven from gravity and spontaneous slick collection. What's more, the mesh still exhibits a separation efficiency above 95% and this collection system can be reused and the oil collection rate can reach >96%.

[a]College of Chemical and Biological Engineering, Taiyuan University of Science and Technology, Taiyuan, Shanxi 030024, China. E-mail: yuezhongzhang@sina.cn

[b]College of Materials Science and Engineering, Taiyuan University of Science and Technology, Taiyuan, Shanxi 030024, China. E-mail: liubaosheng@tyut.edu.cn

† Electronic supplementary information (ESI) available. See DOI: 10.1039/c8ra06059b

Experimental

Materials

Stainless steel meshes (400 mesh, Taitong Metal Mesh Ltd., China) with a size of 35 mm × 35 mm was used as the substrate. Zinc acetate dehydrate, zinc nitrate hexahydrate, ammonia and stearic acid ($C_{18}H_{36}O_2$) were used as received (analytical grade, Sinopharm Chemical Reagent Co., Ltd., China).

Sample preparation

The superhydrophobic and superoleophilic stainless steel mesh was prepared by the following procedures: (1) pretreatment for substrate. The stainless steel mesh was cleaned ultrasonically in ethanol and distilled water respectively to remove the dirt on the surface. (2) Preparing ZnO microstructures. The stainless steel mesh was immersed in a 40 mmol L^{-1} aqueous zinc acetate ethanol solution for 5 min and dried in air, and then it was annealed at 350 °C for 30 min to form a ZnO seed layer on the steel mesh substrate. In the next step, the pretreated substrate was immersed vertically in an aqueous solution of zinc nitrate hexahydrate (40 mmol L^{-1}) and ammonium hydroxide (1.0 mol L^{-1}). The solution was heated in an oil bath at 90 °C for 9 h. Then, the mesh was removed from the solutions, washed with deionized water and dried at in air. (3) Modification of stearic acid. The ZnO coated mesh was immersed in a mixed solution of ethanol (15 mL) and stearic acid (0.12 g) for 12 h and finally heated at 100 °C for 1 h. The schematic illustration of the fabrication process is shown in Fig. 1.

Characterization

The morphological structures of the as-prepared mesh surfaces were examined by scanning electron microscopy (SEM, Hitachi S-4800). The BET specific surface areas of the meshes were characterized by an Auto-IQ-MP (Quantachrome Instruments) using N_2 adsorption at 77 K. The infrared spectra of the samples were investigated by using Fourier transform infrared spectrometry (FTIR, Nicolet iN10). Surface chemical composition of the samples was investigated by X-ray photoelectron spectrometer (XPS, Thermoelectron ESCALAB 250). The water and oil contact angles (CAs) were measured with a JC2000C apparatus at ambient temperature. The volume of the individual
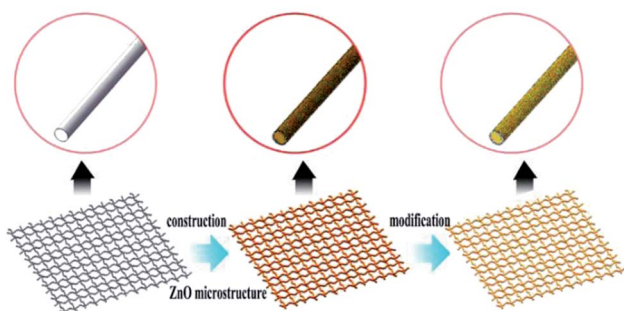
water droplet used in all measurements was 3 μL. The average CA were obtained by measuring the same sample in at least five different positions.

Mechanical durability test

The mechanical durability of the samples was examined by mechanical bending and twisting test and scratch test. The morphology of superhydrophobic meshes after mechanical bending and twisting was investigated. The as-prepared superhydrophobic mesh (30 mm × 30 mm) was placed on sandpaper (#200) with a pressure of 1.09 kPa (100 g force) and as-prepared superhydrophobic mesh was selected to be moved back tangentially on the sandpaper in two orthogonal directions. The distance of each movement was 10 cm for each direction. The evolution of WCA was measured for different cycles.

Corrosion resistances measurement

The corrosion resistances of the samples were investigated by electrochemical measurements in 3.5 wt% NaCl solution at 25 °C. Electrochemical measurements were conducted in a three-electrode cell using a platinum counter electrode and an Ag/AgCl reference electrode. Potentiodynamic polarization curves were measured in with the scanning rate of 0.5 mV s^{-1}.

Oil/water separation and floating oil collection test

The oil/water separation measurement was performed on a homemade equipment (Fig. 7a). The oil/water mixtures (50%, v/v) were poured onto the as-prepared superhydrophobic and superoleophilic mesh. The floating oil collection test was performed on a homemade oil skimmer (Fig. 8a), in which the as-prepared mesh was mounted on the open end of a bottle using a cap with a hole of 13 mm and the steel beads are used to overcome buoyancy to increase the contact area between the mesh and the floating oil. The separation or collection efficiency was calculated according to $\eta = (m_1/m_0) \times 100\%$, where m_0 and m_1 are the mass of the oil before and after the separation process, respectively.

Recycling test

The oil/water separation efficiency *versus* the recycle numbers were tested using hexane/water mixture. After oil/water separation, the contaminated mesh was cleaned with alcohol to remove the absorbed oil and rinsed with deionized water. Finally, the cleaned mesh was dried at 60 °C for 40 min and the superhydrophobicity could be recovered.

Results and discussion

Surface morphology and chemical composition analysis

Typical SEM images at different magnifications of the stainless steel meshes surface are shown in Fig. 2. Fig. 2a and b indicate the pristine stainless steel mesh with an average wire diameter of approximately 40 μm to form the reticulated structure with pore size about 50 μm. The wire surface of the pristine mesh is smooth (Fig. 2c). The ZnO-coated mesh retains its original pore
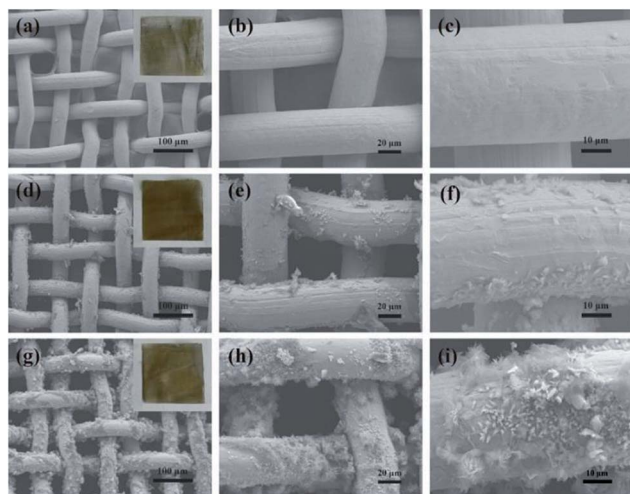

Fig. 1 Schematic illustration of the fabrication process of superhydrophobic stainless steel mesh.

Fig. 2 SEM images of the stainless-steel meshes surface: (a–c) pristine mesh, (d–f) ZnO coated mesh and (g–i) superhydrophobic stainless steel mesh, respectively.

Fig. 3 XPS results for the superhydrophobic stainless steel mesh surface: (a) survey spectrum, (b) Zn 2p high-resolution spectrum, (c) C 1s high-resolution spectrum, and (d) O 1s high-resolution spectrum.

size and wire diameter without apparent variation (Fig. 2d and e). However, regular microstructures are formed on the stainless steel wire surface. The corresponding high magnification SEM image reveals that the microstructure consists of irregular rod-like with a diameter ranging from 300 nm to 400 nm and length of 2–4 μm (Fig. 2f). After modification with the stearic acid, more micro–nano protrusions are observed on superhydrophobic stainless steel mesh (Fig. 2g). The magnified SEM images (Fig. 2h and i) show the randomly distributed clustered structure consisting of nanosheets. Furthermore, the specific surface areas of the meshes were characterized and N_2 adsorption isotherms at 77 K were shown in Fig. S1.† The BET surface areas of pristine mesh, ZnO coated mesh and superhydrophobic mesh were calculated to 0.331, 0.968 and 4.555 m^2 g^{-1} respectively. The increase in specific surface area contributes to increased surface roughness after ZnO construction and modification process. This constructed micro- and nano-scale hierarchical structures are essential for endowing superhydrophobicity.

The constructed ZnO microstructure and the presence of low surface energy chemical functional groups after modification process are supported by the XPS and FTIR spectra. Fig. 3 shows XPS results of the superhydrophobic stainless steel mesh surface. The existence of elements Zn, O, and C is confirmed from the survey XPS spectra (Fig. 3a). The Zn 2p3/2 and 2p1/2 peaks (Fig. 3b) are centered at 1022.1 and 1045.3 eV, respectively, which are assigned to Zn^{2+}.[26] The high-resolution C 1s spectrum (Fig. 3c) can be fitted by three peaks respectively centered at 288.7 eV, 285.2 eV and 284.7 eV, which can be assigned to –COO–, –CH$_2$, and –CH$_3$.[27,28] The high-resolution O 1s spectrum (Fig. 3d) can be fitted by two peaks, respectively centered at 533.3 eV and 531.7 eV. These weak peaks can be assigned to –COO[29] and O^{2-} ions within a ZnO matrix,[20,30] which indicated that ZnO microstructures are constructed and stearic acid is successfully modified on the stainless steel mesh surface. This is further confirmed by FT-IR (Fig. 4).
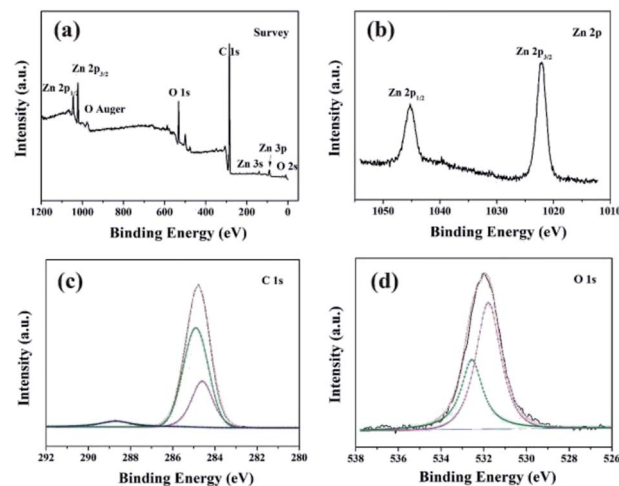
Fig. 4 shows the FITR spectra of modified stainless-steel mesh surface and FTIR spectrum of pristine stainless steel mesh and ZnO coated stainless steel mesh are also given for comparison. In the case of pristine stainless steel mesh, the characteristic absorption bands in the range of 3570–3900 cm^{-1} and 1900–2400 cm^{-1} are assigned to the stretching vibrations of O–H and CO_2. The ZnO coated stainless steel mesh shows weak absorption bands at 2920, 2581 and 1534 cm^{-1} assign to the stretching vibration of the symmetric –CH$_2$ stretch, the asymmetric –CH$_2$ stretch and bending vibration of the antisymmetric carboxylate ion (–COO–).[31,32] These weak peaks can be assigned to adsorbed zinc acetate. Compared with the ZnO coated mesh, the peaks at 1460 and 1397 cm^{-1} are observed for the superhydrophobic mesh. The strong characteristic peak at 1460 cm^{-1} is corresponding to the chelating coordination of zinc with stearic acid to form CH$_3$(CH$_2$)$_{16}$COO–Zn,[33] indicating that the stearic acid modification results in a bond formation with ZnO. The peak at 1390 cm^{-1} are assigned to the bending vibration of –CH$_3$.[34] What's more, the transmittance of the peaks at 2920
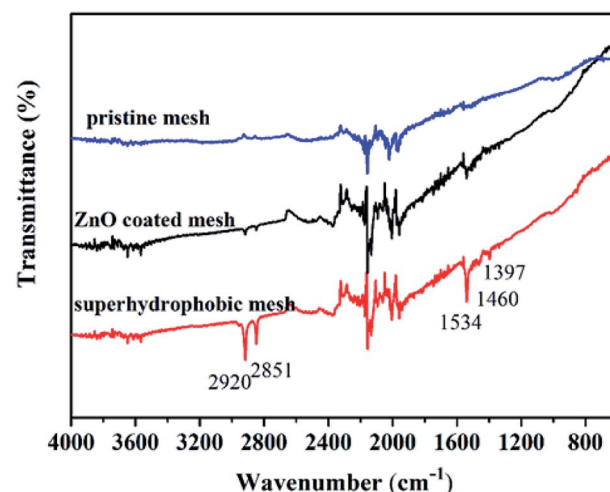

Fig. 4 FTIR spectra of stainless steel meshes.

and 2850, 1534 cm^{-1} of the superhydrophobic mesh obviously enhanced, which can be attributed to modified stearic acid. A combination of SEM, XPS and FTIR results show that the micro- and nano-scale hierarchical structures are constructed and low surface energy materials are successfully modified on the stainless steel mesh surface through this facile approach.

Surface wettability analysis

The surface wettability of the stainless steel meshes was evaluated by measuring the water and oil contact angle, and corresponding results are shown in Fig. 5. As shown in Fig. 5a and d, the pristine stainless steel mesh shows the amphiphilic nature with water and oil contact angle is 69° and 0°. After the ZnO microstructures construction process, the ZnO coated stainless steel mesh exhibits special wettability. The water droplet keeps a highly spherical shape on the ZnO coated mesh while the oil droplet quickly spreading, the corresponding water contact angle is 122° and oil contact angle is about 0° (Fig. 5b and e). The high hydrophobicity can be attributed to absorbed hydrophobic functional groups and ZnO microstructures. Fig. 5c and f show water droplets and oil droplets on ZnO coated stainless steel mesh followed by stearic acid modification, the water contact angle of 156° and oil contact angle of about 0° illustrates the prepared stainless steel meshes endowed superhydrophobic and superoleophilic properties simultaneously. Owing to connected the rough hierarchical structures and intrinsic hydrophobicity of stearic acid, the prepared mesh shows special wettability. As a proof of the special wettability, the photograph of a water droplet (Methylene blue colored) and an oil droplet

(Sudan III colored) on the superhydrophobic and super-oleophilic stainless steel mesh surfaces is shown in Fig. 5g. It is observed that the red oil droplet spreads and water droplet keeps a sphere, so the surface shows good water repellent and oleophilic property.

Mechanical durability, chemical stability and corrosion resistant property

The durability and stability such as mechanical durability, chemical stability under acid and alkali conditions and corrosion resistance property are important indexes to evaluate the value of superhydrophobic and superoleophilic mesh for practical applications. The mechanical durability of the superhydrophobic mesh was examined by mechanical bending and twisting test and scratch test. The morphology of superhydrophobic mesh after mechanical bending and twisting is investigated and showed in Fig. 6a. The original morphology can be well maintained and no obvious micro and nanostructures fall off. What's more, the evolution of the water contact angle *vs.* friction times is shown in Fig. 6b. The water contact angle decreases from 156° to 140° within 8 frictions, and no significant change of water contact angle changes are observed with increasing friction time after 10 frictions. Chemical stability of the superhydrophobic mesh was evaluated by characterizing the contact angles of droplets with different pH values (Fig. 6c). The mesh can well maintain its superhydrophobic property, and water contact angles are all higher than 150° under the different pH from 1 to 14. Thus, as-prepared mesh has relatively good durability and stability.

The corrosion resistance of the superhydrophobic mesh was investigated in 3.5 wt% NaCl solution and comparing those of the pristine mesh. Fig. 6d shows the potentiodynamic
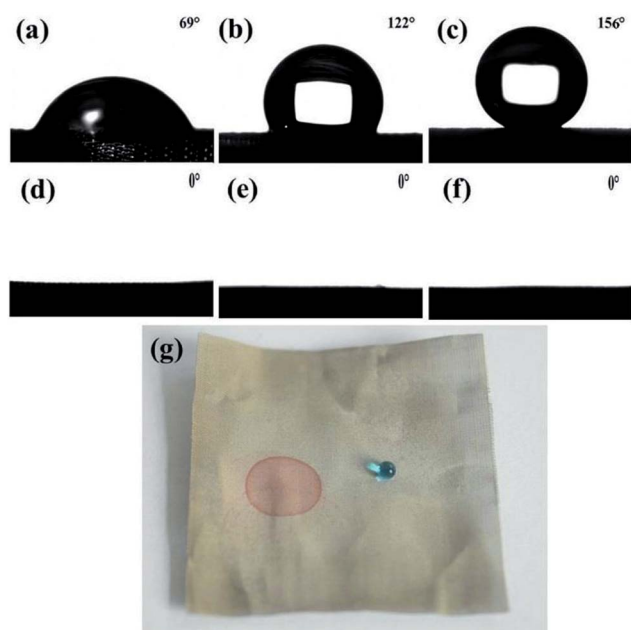

Fig. 5 Digital photographs of water droplet (3 μL) shapes on stainless steel meshes surfaces: (a) pristine mesh, (b) ZnO coated mesh and (c) superhydrophobic mesh; digital photographs of *n*-hexane droplet (3 μL) shapes on stainless steel meshes surfaces: (d) pristine mesh, (e) ZnO coated mesh and (f) superhydrophobic mesh; (g) photograph of Methylene blue colored water droplet and Sudan III colored oil droplet on the modified stainless steel mesh surfaces.
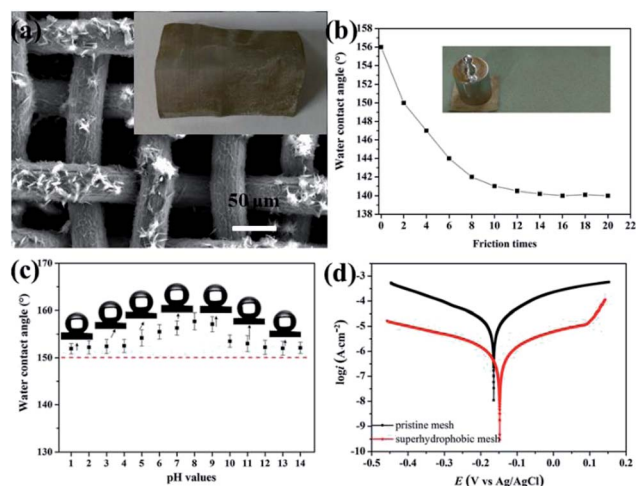

Fig. 6 The mechanical durability, chemical stability and anti-corrosion property of superhydrophobic stainless steel mesh. (a) SEM images of meshes after mechanical bending and twisting (inset: a digital photograph of the bended mesh), (b) influences of friction times on water contact angles, (c) the contact angles of droplets with different pH values (pH = 1–14) and (d) potentiodynamic polarization curves of pristine and superhydrophobic mesh.

polarization curves of pristine and superhydrophobic meshes. The corrosion potential E_{corr} of the superhydrophobic mesh (-0.148 V) shifts about 20 mV in the positive direction as compared to that of pristine mesh (-0.165 V). The corrosion current density i_{corr} of the superhydrophobic mesh decreases to one-twelfth of that for pristine mesh from 2.032×10^{-5} A to 1.698×10^{-6} A. As well known, a higher corrosion potential and a lower corrosion current density correspond to better corrosion resistance and a lower corrosion rate.[35] Obviously, the superhydrophobic mesh possesses better corrosion resistance. The corrosion resistance of the superhydrophobic mesh can be attributed to the following reason:[27,35–37] the trapped air by the hierarchical structure acts as a physical barrier and such an air barrier not only can prevent corrosive ions from penetrating but also inhibit the electron transfer between the corrosive medium and the stainless steel mesh.

Oil/water separation and floating oil collection performance

In view of the above-demonstrated superwettability, the superhydrophobic and superoleophilic stainless steel mesh is predicted to be useful for oil–water mixture separation. As a proof of concept, oil/water mixture separation experiment of the as-prepared the superhydrophobic and superoleophilic mesh is performed and the separation procedure is shown in Fig. 7a and b and Movie S1.† The as-prepared mesh is fixed between two fixtures mounted glass tubes. A colored hexadecane–water mixture is poured along the glass tube. The hexadecane is selectively filtered while the water is hindered, which indicates that separation of oil/water mixtures is successfully achieved using the as-prepared mesh. In order to evaluate the performance of the as-prepared mesh in practical applications, a series of oil–water mixtures including 2,2,4-trimethyl pentane, petroleum ether, carbon tetrachloride and peanut oil were tested and corresponding separation efficiency is shown in Fig. 7c. The as-prepared mesh exhibits the separation efficiency above 95.0% for all five oil–water mixtures. Furthermore, the as-prepared mesh still retain the high separation efficiency above 95.1% after 10 separation cycles for the hexane–water mixture (Fig. 7d), indicating good recyclability of the as-prepared mesh. Considering the industrial application and offshore oil spill, oil/water separation meshes are often needed to be used in acidic or alkaline and sea water environments. Oil–water separation efficiency of the mesh in harsh environments was tested. The mesh exhibits high separation efficiencies above 95.0% for all the corrosive solutions and oil (n-hexane) mixtures (Fig. 7e), revealing outstanding environmental stability. These results show that as-prepared meshes has further potential applications in complex industrial oily wastewater treatment.

To expand the scope of application of the superhydrophobic and superoleophilic mesh, an oil skimmer device based on as-prepared mesh is design for floating oil collection *in situ*. The collection and removal processes of floating oil using the as-prepared oil skimmer are shown in Fig. 8a and Movie S2.† The part of mounted superhydrophobic and superoleophilic mesh always maintains contact with oil phase and water phase throughout the whole collection process. Once the oil skimmer is put into the oil–water mixture surface, the mesh is wetted
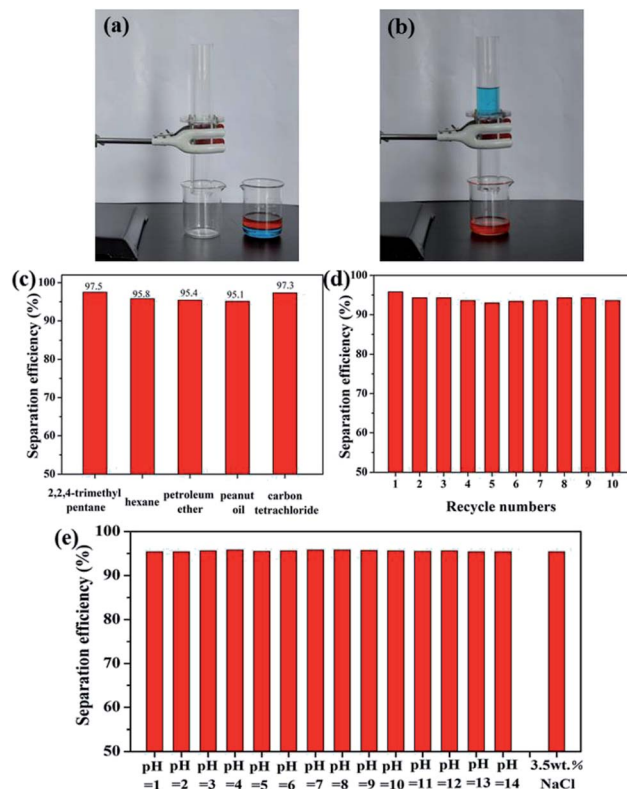

Fig. 7 Oil/water separation of superhydrophobic and superoleophilic stainless steel mesh (water is dyed with methylene blue and oil is dyed with Sudan III to enhance the visual effect): (a) before separation; (b) after separation; (c) the separation efficiency of the oil/water mixtures; (d) the oil/water separation efficiency *versus* the recycle numbers by taking the hexane–water mixture as an example and (e) the separation efficiency of the mesh for separating *n*-hexane and various corrosive solution mixtures.

immediately by floating oil and floating oil pass through the mesh fast and flow into the bottom of the oil skimmer. The oil skimmer with opposite wetting property to oils and water mesh endows an automatic collection and removal process of the floating oil. When the amount of the floating oil was less than the maximum capacity of the oil skimmer, the floating oil collection efficiency is always above 96% and even reaches to 96.9% for petroleum ether (Fig. 8b). Compared with as-prepared oil skimmer, the separation efficiency and collection method of reported superhydrophobic materials for floating oil collection are listed in Table 1. What's more, the oil skimmer exhibits high floating oil collection efficiency always remaining at above 95.2% after 5 times collection for the hexane–water mixture (Fig. 8c), which indicated the good recyclability of the as-prepared mesh.

Oil–water separation mechanism

According to the SEM, XPS and FT-IR analysis, the combined effect of the hierarchical structures and low surface energy endow the stainless steel mesh superhydrophobic and superoleophilic properties. To further explore the oil–water mixture separation mechanism of the superhydrophobic and superoleophilic stainless steel mesh, the super-wettability models are established and shown in Fig. 9. For these models, the pores of
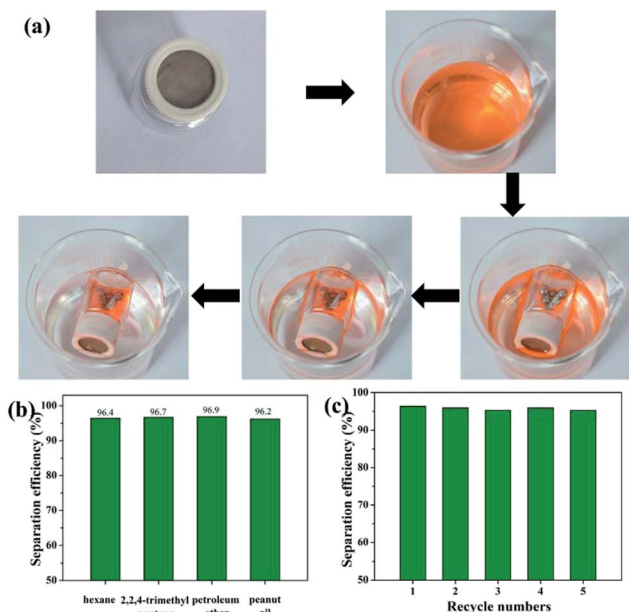
Fig. 8 Removal and collection processes of the floating oil using the oil skimmer: (a) removal and collection processes of hexane. (b) The separation efficiency of the oil skimmer for different oils, (c) the oil/water separation efficiency *versus* the recycle numbers by taking the hexane as an example.

stainless steel mesh are assumed to be arranged in a regular square array. According to Laplace equation,[42] superhydrophobic mesh (Fig. 9a) suffers from the positive intrusion pressure ($\Delta P_{\text{capillarity}} > 0$) due to negative capillary effect, which result in the water was repelled. In contrast, oil can permeate the mesh due to the negative intrusion pressure ($\Delta P_{\text{capillarity}} < 0$) from capillarity of the micropore. Furthermore, oil is trapped in the rough structures during the separation process, which resulted in increase of the repulsive force between water and
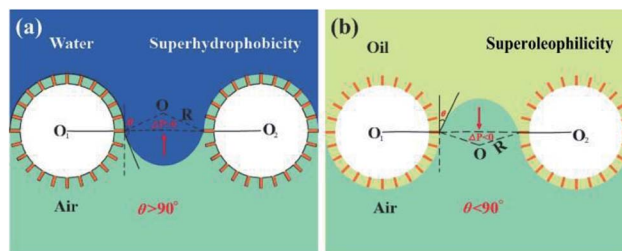

Fig. 9 Schematic illustration of liquid-wetting modes of the superhydrophobic and superoleophilic mesh: (a) water wetting model of the coated mesh. (b) Oil wetting model of the coated mesh. O is the center of the spherical cap of the meniscus; O_1 and O_2 are the cross-section center of the mesh.

mesh.[43] Therefore, the superhydrophobic and superoleophilic properties facilitate the separation of oil–water mixtures efficiently. Similarly, the mesh mounted on oil skimmer is also subjected to similar intrusion pressure. Therefore, the oil skimmer is able to realize floating oil collection.

Conclusions

In conclusion, ZnO coated superhydrophobic and superoleophilic stainless steel meshes is prepared through a facile and inexpensive chemical immersion growth and subsequent surface modification with WCA of 156° and OCA of 0°. Furthermore, as-prepared mesh could be employed to separate various oil–water mixtures driven by gravity with an oil–water separation efficiency larger than 95%. Meanwhile, a new oil skimmer based on the as-prepared mesh is proposed to spontaneous collect floating oil with oil collection efficiency above 96%. Importantly, the oil–water separation efficiency and floating oil collection can retain their high efficiency even after 5 cycles. This facile and novel oil skimmer based as-prepared stainless steel mesh combined with good mechanical

Table 1 Comparison of various superhydrophobic materials for floating oil collection

Substrate materials	WCA (°)	Oils	Separation efficient (%)	Collection method	Ref.
Copper mesh	157	Hexadecane	97.5	Manual	38
		Gasoline	96.3		
		Toluene	96.9		
		Mineral oil	95.7		
Fabrics	158	Hexadecane	99.98	Manual	39
		Cyclohexane	99.96		
		Petroleum ether	99.98		
		Vegetable oil	99.98		
		Soybean oil	99.97		
		Vacuum pump oil	99.95		
40 mesh stainless steel	144	Oil	—	Automatic	40
Cu foam	151	Hexane	98.5	Automatic	41
		Hexadecane	97.6		
		Mineral oil	94.3		
		Corn oil	91.9		
Stainless steel mesh	156	Hexane	96.4	Automatic	This work
		2,2,4-Trimethyl pentane	96.7		
		Petroleum ether	96.9		
		Peanut oil	96.2		

durability, chemical stability and corrosion-resistant properties, which makes it an ideal candidate for application in floating oil collection on the ocean and stable oily wastewater.

Conflicts of interest

There are no conflicts to declare.

Acknowledgements

Notes and references

1 M. M. Pendergast and E. M. V. Hoek, *Energy Environ. Sci.*, 2011, **4**, 1946.
2 R. P. Schwarzenbach, T. Egli, T. B. Hofstetter, U. von Gunten and B. Wehrli, *Annu. Rev. Environ. Resour.*, 2010, **35**, 109136.
3 M. A. Shannon, P. W. Bohn, M. Elimelech, J. G. Georgiadis, B. J. Marinas and A. M. Mayes, *Nature*, 2008, **452**, 301310.
4 Y. Yang, H. Wang, J. X. Li, B. Q. He, T. H. Wang and S. J. Liao, *Environ. Sci. Technol.*, 2012, **46**, 6815.
5 Y. Dou, D. Tian, Z. Sun, Q. Liu, N. Zhang, J. H. Kim, L. Jiang and S. X. Dou, *ACS Nano*, 2017, **11**, 2477.
6 S. Y. Zhang, F. Lu, L. Tao, N. Liu, C. R. Gao, L. Feng and Y. Wei, *ACS Appl. Mater. Interfaces*, 2013, **5**, 11971.
7 Z. Xu, D. Y. Jiang, Z. B. Wei, J. Chen and J. F. Jing, *Appl. Surf. Sci.*, 2018, **427**, 253.
8 S. K. Hubadillah, P. Kumar, M. H. D. Othman, A. F. Ismail, M. A. Rahman and J. Jaafar, *RSC Adv.*, 2018, **8**, 2986–2995.
9 G. N. Ren, Y. M. Song, X. M. Li, Y. L. Zhou, Z. Z. Zhang and X. T. Zhu, *Appl. Surf. Sci.*, 2018, **428**, 520.
10 Z. Shi, W. Zhang, F. Zhang, X. Liu, D. Wang, J. Jin and L. Jiang, *Adv. Mater.*, 2013, **25**, 2422.
11 X. Gao, L. P. Xu, Z. Xue, L. Feng, J. Peng, Y. Wen, S. Wang and X. Zhang, *Adv. Mater.*, 2014, **26**, 1771.
12 Z. Xue, S. Wang, L. Lin, L. Chen, M. Liu, L. Feng and L. Jiang, *Adv. Mater.*, 2011, **23**, 4270.
13 K. Kota, G. Kwon, W. Choi, J. M. Mabry and A. Tuteja, *Nat. Commun.*, 2012, **3**, 1025.
14 H. Yoon, S. H. Na, J. Y. Choi, S. S. Latthe, M. T. Swihart, S. S. Al-Deyab and S. S. Yoon, *Langmuir*, 2014, **30**, 11761.
15 F. Zhang, W. Zhang, Z. Shi, D. Wang, J. Jin and L. Jiang, *Adv. Mater.*, 2013, **25**, 4192.
16 H. J. Cao, J. Y. Fu, Y. Liu and S. G. Chen, *Colloids Surf., A*, 2018, **537**, 294.
17 Z. Xu, D. Y. Jiang, Z. B. Wei, J. Chen and J. F. Jing, *Appl. Surf. Sci.*, 2018, **427**, 253.

18 R. Gao, Q. Liu, J. Wang, J. Y. Liu, W. L. Yang, Z. Gao and L. H. Liu, *Appl. Surf. Sci.*, 2014, **289**, 417.
19 J. Yong, F. Chen, Q. Yang, Y. Fang, J. L. Huo and X. Hou, *Chem. Commun.*, 2015, **51**, 9813.
20 Y. Huang, D. K. Sarkar and X. G. Chen, *Appl. Surf. Sci.*, 2015, **327**, 327.
21 E. Velayi and R. Norouzbeigi, *Appl. Surf. Sci.*, 2018, **441**, 156.
22 H. Lu, X. Y. Zhai, W. W. Liu, M. Zhang and M. Guo, *Thin Solid Films*, 2015, **586**, 46.
23 X. F. Wang, H. Lu, W. W. Liu, M. Guo and M. Zhang, *Ceram. Int.*, 2017, **43**, 6460.
24 D. Nesheva, V. Dzhurkov, I. Stambolova, V. Blaskov, I. Bineva, J. M. C. Moreno, S. Preda, M. Gartner, T. H. Vasileva and M. Shipochka, *Mater. Chem. Phys.*, 2018, **209**, 165.
25 D. G. Ayana, R. Ceccato, C. Collini, L. Lorenzelli, V. Prusakova and S. Dirè, *Mater. Res. Bull.*, 2013, **48**, 25.
26 H. Li, M. J. Zheng, S. D. Liu, Li. Ma, C. Q. Zhu and Z. Z. Xiong, *Surf. Coat. Technol.*, 2013, **224**, 88.
27 L. J. Li, Z. Y. Zhang, J. L. Lei, J. X. He, R. Lv, N. N. Li and F. S. Pan, *Corros. Sci.*, 2014, **85**, 174.
28 N. E. Zaffiropoulos, P. E. Vickers and C. A. Baillie, *J. Mater. Sci.*, 2003, **38**, 3903.
29 G. L. Fisher, A. V. Walker, A. E. Hooper, T. B. Tighe, K. B. Bahnck, H. T. Skriba, M. D. Reinard, B. C. Haynie, R. L. Opila, N. Winograd and D. L. Allara, *J. Am. Chem. Soc.*, 2002, **124**, 5528.
30 K. G. Saw, K. Ibrahim, Y. T. Lim and M. K. Chai, *Thin Solid Films*, 2007, **515**, 2879.
31 L. Li, H. Q. Yang, J. Yu, Y. Chen, J. H. Ma, J. Y. Zhang, Y. Z. Song and F. Gao, *J. Cryst. Growth*, 2009, **311**, 4199.
32 K. Yang, H. B. Peng, Y. H. Wen and N. Li, *Appl. Surf. Sci.*, 2010, **256**, 3093.
33 H. Li, M. Zheng, L. Ma, C. Zhu and S. Lu, *Mater. Res. Bull.*, 2013, **48**, 25.
34 Y. Feng, S. Chen and Y. Frank Cheng, *Surf. Coat. Technol.*, 2018, **340**, 55.
35 P. Wang, D. Zhang, R. Qiu and B. Hou, *Corros. Sci.*, 2001, **53**, 2080.
36 E. Velayi and R. Norouzbeigi, *Appl. Surf. Sci.*, 2017, **426**, 674.
37 Y. Shi, Y. Wu, X. Feng, Y. Wang, G. Yue and S. Jin, *Appl. Surf. Sci.*, 2016, **367**, 493.
38 G. Ren, Y. Song, X. Li, Y. Zhou, Z. Zhang and X. Zhu, *Appl. Surf. Sci.*, 2018, **428**, 520.
39 C. L. Zhang, P. Li and B. Cao, *Ind. Eng. Chem. Res.*, 2018, **57**, 329.
40 Y. Xu, M. Liu, H. Li and A. Wali, *Surf. Coat. Technol.*, 2017, **325**, 661.
41 J. L. Song, Y. Lu, J. Luo, S. Huang, L. Wang, W. L. Xu and I. P. Parkin, *Adv. Mater. Interfaces*, 2015, **2**, 1500350.
42 R. Zhou, S. D. Lin, F. Shen, S. Y. Khew and M. H. Hong, *Surf. Coat. Technol.*, 2018, **348**, 73.
43 E. S. Zhang, Z. J. Cheng, T. Lv, Y. H. Qian and Y. Y. Liu, *J. Mater. Chem. A*, 2015, **3**, 13411.